

Prediction of corroded reinforced concrete beam deflection using a metaheuristic optimized least squares support vector regression

Assoc.Prof. Duc-Hoc Tran ^{1,2*}, Email: tdhoc@hcmut.edu.vn, Phone: +84-988922999
PhD Student. Thi-Cam Tien Ngo ^{1,2}, Email: ntctien.sdh241@hcmut.edu.vn, Phone: +84-765820060

* *Corresponding author*

¹ Faculty of Civil Engineering, Ho Chi Minh City University of Technology (HCMUT), 268 Ly Thuong Kiet Street, District 10, Ho Chi Minh City, Vietnam.

² Vietnam National University Ho Chi Minh City, Linh Trung Ward, Thu Duc City, Ho Chi Minh City, Vietnam.

Abstract

The study develops a machine learning technique to predict structural deformation in corroded reinforced concrete (RC) beams, enabling a more accurate assessment of building structural health and potential long-term degradation risks. The method combines least squares support vector regression (LSSVR) with an innovative opposition sea-horse optimizer (OSH) to handle the nonlinear and multivariable aspects of deflection prediction. The OSH optimizer enhances the LSSVR's performance by fine-tuning its learning process. The research validated the predictive approach by analyzing 150 samples from deteriorating residential structures in southern Vietnam, employing cross-validation techniques to verify the model's precision and reliability. The OSH-LSSVR approach significantly surpasses traditional predictive models, including artificial neural networks, multivariate adaptive regression splines, and support vector regression. Empirical evaluation reveals exceptional performance metrics, with a root-mean-square error of 1.896 mm, mean absolute error of 1.198 mm, and a coefficient of determination of 0.891, underscoring its advanced predictive capabilities. The developed model provides civil engineers with an advanced tool for predicting RC beam deflection, opening new avenues for research in structural optimization, early warning systems, and proactive safety strategies.

Keywords: Corroded reinforced concrete, beam deflection, corroded reinforced concrete, least squares support vector regression, sea-horse optimizer.

1 Introduction

Corrosion gradually weakens enhanced and tensioned concrete by eroding the steel's cross-sections and damaging the crucial steel-concrete interface, thus undermining the materials' structural integrity [1]. This degradation manifests as cracking, spalling, and delamination, compromising the structure's functionality and leading to deformities such as abnormal bending or sagging of the concrete structural elements [2, 3]. Both concrete and steel components are susceptible to deterioration from environmental factors such as moisture, carbon dioxide,

36 chloride, and sulfate infiltration [4]. Corrosion in RC structures, primarily caused by the
37 penetration of chloride ions and carbonation of concrete, poses a significant risk to their
38 longevity and safety [5].

39 Carbonation lowers the concrete's pH, making steel reinforcement vulnerable to corrosion,
40 while chloride ions disrupt the protective oxide layer, causing localized corrosion [6]. This
41 results in rust expansion, which causes internal pressures that crack and delaminate concrete,
42 leading to accelerated degradation, costly repairs, reduced service life, and potential structural
43 failure [7]. In coastal regions with high chloride exposure, the electrochemical reaction speeds
44 up the rusting of steel reinforcements within concrete structures. This corrosion reduces the
45 cross-sectional area of the steel, thereby decreasing the load-bearing capacity of the reinforced
46 concrete elements. This corrosion leads to internal stresses, cracking, spalling, and concrete
47 delamination, posing serious safety hazards [8]. Therefore, to ensure structural durability and
48 functionality, quality materials and protective coatings must be used, and regular inspections
49 and maintenance must be conducted to enhance safety and reduce costs over time [9, 10].

50 Reinforced concrete apartment buildings are the preferred housing in densely populated
51 Vietnamese cities, but aging over 50 years in Ho Chi Minh City, this aging process raises
52 concerns about the quality and structural stability of these buildings. Prolonged exposure to
53 environmental conditions and natural aging processes like steel corrosion and concrete spalling
54 have led to widespread building deterioration, challenging structural engineers and urban
55 planners to maintain safety and stability while also heightening residents' concerns about safety
56 and quality of life [11]. Corrosion caused by the infiltration of carbonate and chloride is a
57 significant problem for RC structures, resulting in damage to the concrete and compromised
58 bond strength [12]. Assessing the remaining load-bearing capacity of deteriorated reinforced
59 concrete elements requires a comprehensive analysis of their mechanical properties,
60 deformation characteristics, and structural stability [13]. Such rigorous assessment is critical
61 for developing targeted maintenance and rehabilitation approaches that ensure long-term
62 structural performance and safety.

63 Extensive research using 3D finite element modeling has enhanced our understanding of
64 reinforcement corrosion and its impact on the structural integrity of RC components, including
65 assessments of flexural strength in corrosion-damaged beams [14]. Additionally, modeling the
66 bond between corroded steel bars and the surrounding concrete is crucial for understanding the
67 impact of corrosion on the structural performance of RC elements [15]. However, These models
68 often lack generalizability and fail to mimic real-world corrosion accurately, as laboratory
69 experiments use accelerated processes that don't reflect natural, long-term deterioration [16].

90 The discrepancy between theoretical research and real-world aging RC structures raises
91 concerns about practical applicability, necessitating efficient, cost-effective, and realistic
92 modeling approaches.

93 Traditional methods like 3D finite element modeling are resource-intensive, whereas
94 machine learning offers a quicker, data-driven approach to analyzing the residual strength of
95 corroded RC structures, incorporating environmental factors [17-19]. This reduces research
96 time and costs while maintaining accuracy, facilitating proactive maintenance and retrofitting.
97 Machine learning provides the opportunity to enhance the safety and resilience of corroded
98 reinforced concrete structures because it enables a more accurate analysis and prediction of
99 structural deterioration [15, 20].

100 The increasing complexity of engineering challenges has driven the advancement of
101 machine learning techniques, demonstrating remarkable potential in providing sophisticated
102 predictive solutions for intricate real-world technical problems [21]. Machine learning model
103 effectiveness critically hinges on precise hyperparameter configuration, rendering their
104 optimization a complex and nuanced computational challenge [22]. Suykens, J. A., et al. [23],
105 pioneered least squares support vector regression (LSSVR) as an innovative approach to
106 address inherent constraints in traditional support vector machine methodologies, offering a
107 more refined computational framework for predictive modeling. By integrating the least
108 squares (LS) method, LSSVR improves the model's functionality and performance through a
109 reduction in computational complexity. Specifically, the LS in LSSVR substitutes inequality
110 constraints with equality constraints, which simplifies the solution of the linear Karush-Kuhn-
111 Tucker system. The modifications to LSSVR significantly reduce its computational demands,
112 making it highly efficient for handling small to medium-sized datasets. Specifically, small-sized
113 datasets include fewer than 1,000 samples and medium-sized datasets contain between 1,000
114 and 10,000 samples [24]. LSSVR excels with small to medium-sized datasets by using linear
115 equations to simplify computation and enhance efficiency, making it ideal for computationally
116 demanding predictive tasks without requiring large data volumes. The seahorse optimizer (SHO)
117 optimization algorithm, introduced by [25], emulates the natural behaviors of seahorses and has
118 demonstrated robustness in tuning hyperparameters and solving global optimization problems
119 [26]. SHO's adaptability and straightforward approach have rendered it an advantageous option
120 for enhancing the performance of LSSVR.

121 This research introduces a seahorse optimizer-enhanced least squares support vector
122 regression (SHO-LSSVR) approach for predicting corroded reinforced concrete beam
123 deflection. The study aims to: (1) develop a hybrid predictive model with superior accuracy; (2)

1.4 validate the model's performance using empirical data and comparative analysis against existing modeling techniques; and (3) investigate critical factors and their optimal configuration to enhance deflection prediction precision.

1.4.2 Literature review

1.4.2.1 Machine learning has become a pivotal approach for forecasting structural deformation in reinforced concrete elements, with diverse methodologies aimed at enhancing predictive accuracy and reliability. Multiple data-driven machine learning techniques were evaluated, comparing single and ensemble models to identify the most effective approaches for structural deflection prediction, as demonstrated by Bai, C., et al. [11] colleagues. Building on these findings, Pham, A.-D., et al. [27] introduced a specialized machine learning approach designed to forecast progressive deflection patterns in damaged reinforced concrete flexural structures, including beams and slabs. Meanwhile, Li, N., et al. [28] evaluated an advanced artificial neural network model for predicting the deflection of reinforced concrete beams, deriving insights from a comprehensive dataset comprising 120 experimental investigations. In subsequent research, Nguyen, N.-M., et al. [29] introduced an advanced least squares support vector regression technique for early-stage deflection forecasting in RC beams, showcasing significant predictive improvements over traditional artificial intelligence and mathematical modeling methods. Machine learning methodologies provide engineers with sophisticated predictive capabilities, enabling more precise assessment of structural behavior and enhancing design optimization for reinforced concrete elements.

1.4.2.2 Assessing the condition of reinforced concrete structures involves employing a comprehensive range of investigative techniques, including both non-invasive and invasive testing approaches to detect and analyze corrosion-related deterioration [13]. Popular NDT methods, such as rebound hammer tests (TCVN 9334:2012) [30], ultrasonic pulse velocity tests (TCVN 9357:2012) [31], ground-penetrating radar, and infrared thermography, are preferred for routine inspections due to their non-invasive nature. However, used individually, destructive testing methods like concrete core drilling and pull-out tests offer direct mechanical insights but may compromise structural integrity (TCVN 3105:2022)[32]. Integrating destructive testing with digital imaging, machine learning, and finite element modeling improves assessment accuracy, ensuring early detection and effective intervention to extend the service life and safety of RC structures in chloride-exposed regions.

1.4.2.3 Researchers commonly utilize empirical mathematical models to predict reinforced concrete beam deflection, calculating initial displacement from applied loads and estimating

137 long-term deformation caused by sustained loading, material creep, and structural shrinkage
138 [33]. However, These formulas often lack precision due to insufficient consideration of various
139 factors like material properties, construction techniques, and environmental conditions, leading
140 to discrepancies in deflection predictions [34]. Advanced techniques like finite element analysis
141 (FEA) and a combination of empirical and advanced methods are necessary for precise
142 deflection predictions and to ensure the integrity and serviceability of RC beams.

143 Artificial intelligence, particularly via artificial neural networks, has greatly improved the
144 precision of deflection predictions for reinforced concrete beams, surpassing traditional civil
145 engineering methods [35]. Kaczmarek, M. and Szymańska, A. [36] used artificial neural
146 networks to forecast deflections in reinforced concrete beams under different loading conditions
147 with notable precision. Similarly, Mohammadhassani, M., et al. [37] employed artificial neural
148 networks to forecast deflection in high-strength, self-compacting concrete deep beams, refining
149 their predictive model through experimental data derived from eight distinct beam specimens.
150 These findings highlight the potential of AI in enhancing deflection prediction, equipping
151 engineers with an advanced tool for more precise and reliable design and evaluation of RC
152 structures.

153 Mishra, M., et al. [38] investigated the potential of artificial neural networks to predict
154 reinforced concrete beam deflection, utilizing a comprehensive analysis of 122 laboratory test
155 datasets and concentrating on critical determinants including reinforcement percentage, applied
156 load, and concrete tensile strength. Despite its contributions, the model failed to account for
157 numerous additional variables that significantly impact structural deformation. To address this
158 Nguyen, H. D., et al. [39] employed gene expression programming as an alternative
159 methodology to predict beam deflection, analyzing a comprehensive dataset of 108 specially
160 designed experimental specimens. This approach expanded the predictive framework by
161 integrating multiple critical structural parameters, including beam span length, maximum
162 moment, moment of inertia, and mid-span deflection, thereby providing a broader and more
163 detailed evaluation of structural performance. Additionally, Vijayan, D. [40] explored artificial
164 neural network-enabled sensor technologies for real-time reinforced concrete displacement
165 prediction, showcasing innovative monitoring capabilities. These investigations highlight the
166 multifaceted landscape of AI-driven approaches to structural deformation analysis, each
167 methodology offering distinctive perspectives based on carefully selected input variables.

168 The application of machine learning (ML) in predicting deflection in reinforced concrete
169 (RC) components has significantly improved the accuracy and generalizability of results and
170 reduced the interpretability and reliability of the models. Surveys indicate that prior research

frequently neglected the impact of corrosion in aging structures, mainly depending on experimental rather than real-world data. A new inference model using data from corroded RC structures in southern Vietnam improves relevance and accuracy for older buildings, enhancing deflection predictions and result reliability.

3 Machine learning techniques

As mentioned above, the set of individual models, ensemble model, and hybrid AI model have been implemented herein in this study. In particular, the individual models and ensemble models is simulated by the virtual personal-based software SPSS [41]. The hybrid AI model is programmed by using Matlab software [42]. The mathematical definition and description of such individual models, i.e., ANN, support vector machine, Chi-squared automatic interaction detector, Classification and regression trees, and the generalized linear model, have overwhelmingly appeared in many kinds of literature. Hence, such definitions and descriptions are succinct. The ensemble model and the hybrid AI model are presented in detail as follows:

3.1 Ensemble model

The ensemble model is created by combining the best-performing individual techniques [43]. The ensemble yields the first-rank performance among the abovementioned single models. The mathematical expression of the ensemble model can be used ensemble-based function $gen(\cdot)$ obtained by a linear combination of single models as follows.

$$gen_{en}(\cdot) = \sum_{j=1}^N c_j * g(\cdot) \quad (1)$$

where c_j is the average weight of the linear combination; $g(\cdot)$ is the estimated function, which is defined by a specific algorithm implemented in a numerical procedure.

3.2 Hybrid AI model

3.2.1 Least square support vector regression

Introduced by Suykens, J. A., et al. [23], the LSSVR uses Eq. (2) to build a relationship between a response variable and one or more independent variables. In LSSVR, the response variable $y(x)$ is modeled as a linear combination of the transformed inputs, where x represents the input data points in an n -dimensional space, y is the output and ϕ is a transformation that maps the input data into a higher-dimensional feature space. The parameters ω and b represent the weight vector and bias term, respectively, crucial for defining the model's linear decision surface in the transformed feature space.

$$y(x) = \omega^T \phi(x) + b \quad (2)$$

where $x \in R^n$; $y \in R$; R represents the set of real numbers; ϕ is mapping the input data into high-dimensional feature space; ω denotes the weight vector, and b is a bias term.

2.4 For the regression, LSSVR plays a constrained optimization problem, as shown in Eq. (3).

$$2.5 \text{ Minimization of } R(\omega, \varepsilon, b) = \frac{1}{2} \|\omega\|^2 + \frac{1}{2} C \sum_{i=1}^n \varepsilon_i^2 \quad (3)$$

$$2.6 \text{ subject to: } y_i = \omega^T \phi(x_i) + b + \varepsilon_i, i = 1, \dots, n$$

2.7 where C is a user-defined regularization constant, and ε_i denotes the training data error.

2.8 Two tuning parameters (C, γ) are required to determine for improving LSSVR performance.

2.9 Therefore, the following optimization algorithm SHO is applied to define proper setting values

2.10 of C and γ .

2.11 3.2.2 Seahorse optimizer

2.12 The SHO has three key phases: mobility, predation, and breeding. The SHO algorithm starts

2.13 with the initiation of the population as depicted in Eq. (4):

$$2.14 X_i = [x_i^1, \dots, x_i^j, \dots, x_i^D]; x_i^j = \text{rand} \cdot (UB_j - LB_j) + LB_j; i = 1, 2, \dots, NP; j = 1, 2, \dots, D \quad (4)$$

2.15 where X_i is the i^{th} candidate solution in NP size of population; D represents the number of

2.16 dimension in the search space; LB_j and UB_j are the lower and upper bound of the j^{th} variable;

2.17 rand is the randomly generator number within $[0, 1]$.

2.18 In the movement phase, seahorses generate a new solution by moving in spiral or Brownian

2.19 patterns from their current best solution and previous position.

$$2.20 X_i^{\text{new},1} = \begin{cases} X_i^{\text{old}} + \text{Levy}(\lambda) \cdot ((X_{\text{best}} - X_i^{\text{old}}) \cdot x \cdot y \cdot z + X_{\text{best}}); & \text{if } r_1 > 0 \\ X_i^{\text{old}} + \text{rand} \cdot l \cdot \beta_i \cdot (X_i^{\text{old}} - \beta_i \cdot X_{\text{best}}); & \text{otherwise} \end{cases} \quad (5)$$

2.21 where $x = \rho \cdot \cos(\theta)$; $y = \rho \cdot \sin(\theta)$; and $z = \rho \cdot \theta$ are the three-dimensional components to update the

2.22 positions of candidate solutions; θ is arbitrarily selected in the range $[0, 2\pi]$; u and v equal 0.05;

2.23 r_1 is a normal random number; the Levy function is calculated as follows:

$$2.24 \text{ Levy}(\lambda) = s \cdot \frac{w \cdot \sigma}{|k|^{\frac{1}{\lambda}}} \quad (6)$$

2.25 where here λ is randomly selected from the range $[0, 2]$; s equals 0.01; w and k denote random

2.26 numbers in the range $[0, 1]$; σ is computed using Eq. (7). β_i is Brownian motion's random walk

2.27 coefficient. l equals 0.05.

$$2.28 \sigma = \left(\frac{r(1+\lambda) \cdot \sin\left(\frac{\pi\lambda}{2}\right)}{\Gamma\left(\frac{1+\lambda}{2}\right) \cdot \lambda \cdot 2^{\left(\frac{\lambda-1}{2}\right)}} \right) \quad (7)$$

2.29 where Γ is the gamma function.

2.30 In the predation phase, seahorses use their uniquely shaped heads to capture prey with a 90%

231 success rate. The predation operation is mathematically represented by Eq. (8).

$$232 X_i^{new,2} = \begin{cases} \alpha \cdot (X_{best} - rand \cdot X_i^{new,1}) + (1 - \alpha) X_{best}; & \text{if } r_2 > 0.1 \\ (1 - \alpha) \cdot (X_i^{new,1} - rand \cdot X_{best}) + \alpha \cdot X_i^{new,1}; & \text{otherwise} \end{cases} \quad (8)$$

233 here $X_i^{new,1}$ denotes the newly generated solution from the movement phase; r_2 is a random
234 variable ranging between 0 and 1; α decreases with each iteration, as defined by t (current) and
235 T (total iterations) in Eq. (9).

$$236 \alpha = \left(1 - \frac{t}{T}\right)^{\frac{2t}{T}} \quad (9)$$

237 The breeding phase mimics the reproduction process of seahorses, where new solutions are
238 generated by combining the genetic material of parent solutions (fathers and mothers). This
239 phase is mathematically expressed as follows:

$$240 \begin{cases} fathers = X_{sort}^2 \left(1 : \frac{NP}{2}\right); \\ mothers = X_{sort}^2 \left(\frac{NP}{2} + 1 : NP\right); \\ X_k^{child} = r_3 X_k^{father} + (1 - r_3) X_k^{mother}; \quad k = 1, 2, \dots, NP / 2 \end{cases} \quad (10)$$

241 Here, r_3 denotes a random number between 0 and 1, and the fathers and mothers are selected
242 randomly from the sorted population after the predation phase. This study employs the SHO
243 algorithm to optimize the hyperparameters of LSSVR models, specifically the kernel parameter
244 (γ) and the regularization parameter (C), To improve the precision of deflection forecasting for
245 deteriorating reinforced concrete structural elements.

246 3.2.3 The proposal model SHO-LSSVR

247 This subsection introduces the SHO-LSSVR model, a hybrid that combines LSSVR with the
248 SHO algorithm to automatically identify optimal hyper-parameters and construct relationships
249 between data inputs and outputs, as shown in Fig. 1.

250 *<Insert Fig. 1 here>*

251 The historical dataset is split into two segments, with 80% allocated for training and 20%
252 designated for testing. To fine-tune the hyperparameters of the LSSVR, the training portion is
253 further divided into training and validation sets at a 7:3 ratio. This distribution guarantees that
254 70% of the data is used for model training, with the remaining 30% set aside for validation to
255 evaluate the model's effectiveness.

256 4 Experimental results and discussion

2074.1 Data collection and processing

208 This method relies on guidelines from Vietnamese standards to conduct detailed surveys
209 and measure construction parameters. The investigation encompasses a systematic process: (1)
210 documenting structural characteristics and defining project parameters; (2) developing
211 architectural floor plans; (3) conducting structural inspections and dimensional measurements;
212 (4) extracting material samples to evaluate strength and assess beam system deformations; (5)
213 analyzing component surface conditions; and (6) synthesizing collected data for subsequent
214 analytical evaluation. By integrating both destructive and non-destructive testing techniques
215 with meticulous structural parameter documentation, the research establishes a robust
216 framework for in-depth structural analysis. Structural parameters were assessed in Southern
217 Vietnam, focusing on buildings constructed before 1975, over 49 years old by 2024, and those
218 erected after 1975, younger than 49 years, allowing for accurate structural evaluations.

219 The measurement process involves determining the geometric parameters of structural
220 components using specialized tools. The study focuses on critical beam parameters, including
221 cross-sectional dimensions: height (h) from the bottom to the reinforced concrete floor and
222 width (b) representing the beam's lateral extent and span length (L) measured between column
223 centers. Sophisticated non-destructive techniques like ultrasonic and metal detection methods
224 are employed to identify reinforcement configuration and quantity. Reinforcement diameter (\emptyset)
225 is precisely determined by carefully removing the concrete cover and utilizing calipers with
226 1mm accuracy, simultaneously enabling gauging of the thickness of the protective concrete
227 layer (a) and calculation of the total reinforcement cross-sectional area (A_s). Positions for
228 locally destructive measurements and reinforcement area calculations were strategically chosen
229 to address non-destructive methods' limitations in detecting and accurately measuring
230 embedded reinforcement, especially in tightly spaced or deeply covered rebar, enhancing
231 measurement accuracy and reliability as discussed by Drobiec, Ł., et al. [44] and Donkervoort,
232 J. [45].

233 The tensile strength of reinforcement steel (R_s) is assessed through steel tensile testing,
234 while the compressive capacity of concrete (R_b) is evaluated by conducting compression tests
235 on concrete samples. For concrete coring in structural testing, locations are strategically chosen
236 within beams to optimally evaluate load-bearing capacity and stress distribution, typically
237 around one-fifth of the span ($L/5$) from the supports on the lower part of the beam. This position
238 minimizes external disturbances and provides a true representation of the beam's structural
239 integrity. According to TCVN 3105:2022 [46], steel samples for tensile tests are extracted
240 directly from the beams, ensuring they reflect the true quality and condition of the material,

291 unlike manufacturer-supplied samples, which might not accurately represent the in-situ steel's
292 properties. Additionally, the project owner can provide detailed information about the steel's
293 origin and quality.

294 With all the collected input parameters ($L, b, h, a, A_s, R_b, R_s$) collected, the next step uses
295 Etabs software to model and analyze internal forces in the beams. Initial calculations (M_1)
296 assess the immediate impact of the total load, while further measurements evaluate the forces
297 under short-term (M_2) and long-term (M_3) load effects, with the short-term load calculated as
298 70% of M_1 . This approach ensures precise analysis of beam response to various load
299 environments. Fig. 2 from a psychiatric hospital in Ho Chi Minh City, Vietnam, shows
300 reinforced concrete beams with significant sagging, cracking, and signs of concrete spalling
301 and exposed, rusting reinforcement.

302 *<Insert Fig. 2 here>*

303 The study applied comprehensive methods to evaluate concrete strength, adhering to
304 Vietnamese standards: TCVN 9334:2012 [30] for measuring heavyweight concrete's
305 compressive strength via rebound hammer, TCVN 13537:2022 [47] for ultrasonic defect
306 detection in concrete, and TCXDVN 239:2006 [48] for assessing strength in existing structures.
307 According to the TCVN 3118:2022 standard [49], concrete cores for compressive strength
308 testing were extracted through precision drilling and subsequently tested as cylindrical samples
309 in a laboratory. Fig. 3a shows the drilling activity at a psychiatric hospital in Ho Chi Minh City,
310 Vietnam, and Fig. 3b displays the subsequent compression tests on these cores. The study
311 adhered to the TCVN 9356:2012 [50], which specifies the electromagnetic method for
312 measuring the thickness of the protective concrete layer, identifying the position of steel bars,
313 and determining their diameter within concrete structures. Fig. 3c and d illustrate the removal
314 of the outer concrete layer to expose the reinforcement and measure the reinforcement diameter
315 in reinforced concrete beams. Careful concrete removal is essential to avoid compromising the
316 structural integrity of the building.

317 *<Insert Fig. 3 here>*

318 The research evaluates reinforced concrete component deformation and deflection (f) by
319 adhering to TCVN 5574:2018 standards, integrating comprehensive data from field
320 investigations, actual loading conditions, material property analyses, and supplementary
321 documentary evidence [51]. To forecast deflection in deteriorating reinforced concrete beams,
322 the research identified seven critical input variables for comprehensive predictive modeling.
323 For instance, increasing the diameter of the rebar within the permitted range enhanced its load-
324 bearing capacity and distribution capabilities, which in turn reduced the deflection of the beam.

Table 1 presents the influencing factors and deviations, including symbols, minimum and maximum values, average values, and standard deviations, based on 150 data points. The factors in Eq. (11) are crucial for predicting the deflection of the reinforced concrete beam (f).

328

<Insert Table 1 here>

$$f = \frac{5 * L^2}{48} \frac{1}{r} \quad (11)$$

$$\frac{1}{r} = \left(\frac{1}{r}\right)_1 + \left(\frac{1}{r}\right)_2 + \left(\frac{1}{r}\right)_3 \quad (12)$$

$$\left(\frac{1}{r}\right)_i = \frac{M_i}{D}; i = 1, 2, 3 \quad (13)$$

where L represents beam span, while $(1/r)$ indicates the overall bending at a segment resulting from the applied load, which causes deflection. $(1/r)_1$ captures short-term total load curvature, whereas $(1/r)_2$ accounts for short-term permanent and temporary load interactions, and $(1/r)_3$ reflects long-term load effects. The applied moment M and section stiffness D , determined using TCVN 5574:2018 standards [51], were critical in characterizing the structural deformation mechanism.

4.2 Model construction and performance evaluation criteria

The IBM SPSS Modeller [41] was used to evaluate the efficacy of the single prediction techniques and ensemble models. The modeling stream is illustrated in Fig. 4, which consists of five steps: (i) the input data are added to the source node via the cross-validation algorithm and will be processed by the attribute filter node; (ii) the numerical predictor node is used to train data; (iii) the nugget node is applied to validate testing data; (iv) combine models is established via the ensemble node; (v) analytical results are assessed through table and analysis nodes.

346

<Insert Fig. 4 here>

The parameter settings for single and combined data-driven techniques are default values and are selected according to suggested values from the literature [52, 53] and trial and error methods. The selected parameter values aim to ensure that the predictive models are constructed objectively, are easy to operate and deliver satisfactory outcomes in terms of accuracy, utilization, and effectiveness. For instance, in machine learning models employing the RBF kernel, the γ parameter is crucial as it sets the kernel's width, significantly affecting model performance. If γ is set too high, it may lead to overfitting; if too low, underfitting may occur. This study chooses γ based on previous research that identified effective values for comparable

scenarios, as the manuscript details. This method guarantees that the model performs accurately in real-world applications.

Table 2 displays the calibration parameters for comparative models, including the recommended optimal settings [53, 54]. Specifically, the ANN-SVR model's predictions were generated by synthesizing outputs from artificial neural networks and support vector regression using predetermined integration coefficients.

361

<Insert Table 2 here>

This method ensures a more informed decision-making process when choosing models for specific tasks. In our analysis, we employed the coefficient of determination (R^2), root means squared error (RMSE), mean absolute error (MAE), and mean absolute percentage error (MAPE) to evaluate the prediction models comprehensively. These metrics together provide a robust measure of both accuracy and error magnitudes. R^2 indicates the proportion of variance in the dataset that is predictable from the model, with values nearing one, suggesting high accuracy. RMSE gauges the average size of the prediction errors, MAE measures the average absolute errors disregarding their direction, and MAPE, presented as a percentage, evaluates the size of the error relative to the true values. Eqs. (14)–(17) outline the metrics applied, providing a structured method for evaluating the effectiveness of artificial intelligence (AI) based predictive models in this study, thereby enhancing our detailed comprehension of their practical applications.

$$R^2 = 1 - \frac{\sum_{i=1}^n (y_i - p_i)^2}{\sum_{i=1}^n (y_i - \bar{y})^2} \quad (14)$$

$$RMSE = \sqrt{\left(\frac{1}{n}\right) \sum_{i=1}^n (y_i - p_i)^2} \quad (15)$$

$$MAE = \left(\frac{1}{n}\right) \sum_{i=1}^n |y_i - p_i| \quad (16)$$

$$MAPE = \left(\frac{1}{n}\right) \sum_{i=1}^n \left(\frac{|y_i - p_i|}{y_i}\right) * 100 \quad (17)$$

where y_i and p_i represent the observed and forecasted values, respectively; \bar{y} represents the mean of the observed values; and n indicates the overall count of data points.

4.3 Results and Comparison

The SH optimization algorithm, modeled after the behavior of seahorses, optimizes the hyperparameters of the LSSVR to minimize errors while employing five-fold validation to assess the model's performance [55]. Using this technique, the dataset is divided into five

385 subsets for a five-fold cross-validation, where each subset is used once for testing and four
386 times for training across five iterations. Notably, within the training phase, 70% of the data is
387 used for training and 30% for validation. This process is repeated five times, and after each
388 iteration, the average performance data is calculated to provide a reliable assessment of the
389 model's effectiveness.

390 Table 3 summarizes the performance results predicted by models such as artificial neural
391 network (ANN), support vector machine (SVM), chi-squared automatic interaction detector
392 (CHAID), classification and regression trees (CART), generalized linear model (GENLIN), an
393 ensemble model, and hybrid AI. The predictability of these AI techniques is evaluated through
394 standard performance indicators, with cross-validation results displayed in the table for the
395 testing phase. The comparison indicates that the CART model is the most effective among the
396 baseline AI models for predicting the deflection of corroded RC beams, delivering the best
397 RMSE, MAE, MAPE, and R^2 values. Notably, the ensemble model, combining CART and
398 GENLIN, demonstrated even superior overall performance. The average accuracy for
399 predictions in Table 3 indicates that the proposed hybrid AI model outperformed all other AI
400 models in predicting the deflection of corroded RC beams. Fig. 5 further illustrates the
401 evaluation metrics presented in Table 3. The hybrid SHO-LSSVR model achieved the lowest
402 errors among the compared models, with an average R^2 of 0.891 RMSE of 1.896 mm, MAE of
403 1.198 mm, MAPE of 0.547%, and RMSE of 1.896 mm. The proposed AI model enhanced
404 predictive accuracy by 25.3% to 49.9% in MAE and 16.8% to 28.8% in MAPE compared to
405 other methods. The integration of SHO and LSSVR provides structural engineers with an
406 effective tool for assessing and planning the maintenance of aging infrastructure. This method
407 has proven its accuracy in predicting the deflection caused by corrosion in reinforced concrete
408 beams.

409 <Insert Table 3 here>

410 <Insert Fig. 5 here>

411 <Insert Fig. 6 here>

412 The comparative analysis of Fig. 6 reveals the predictive capabilities of various artificial
413 intelligence models in estimating deflection for concrete beams subjected to corrosion. Among
414 the evaluated approaches, the SHO-LSSVR methodology demonstrates remarkable precision.
415 Its performance is distinguished by an exceptional accuracy metric, with maximum absolute
416 deviations reaching a minimal 0.0024 mm a stark contrast to alternative models showing
417 deviations as high as 2.46 mm. The model's reliability is particularly evident in its consistency

across test scenarios. In 64% of the evaluation cases, the SHO-LSSVR approach maintained absolute deviations under 1 mm, a benchmark that significantly outperforms competing models. These competing approaches typically achieved deviation control in less than half of their test instances, typically below 0.5 mm.

Computational time, critical for evaluating model efficiency alongside accuracy, was measured for each model, estimating the deflection of corroded RC beams under consistent hardware conditions. The ANN model had the shortest computing time, taking just 8 seconds. In comparison, SVM, CART, GENLIN, and CHAID required 10 seconds, 10 seconds, 9 seconds, and 9 seconds, respectively, all optimized within the IBM SPSS Modeler. The proposed hybrid SHO-LSSVR model took 1 minute to complete its computations. Although the integration of multiple techniques increases the computational time, this additional time is justified by the significant improvements in prediction accuracy offered by the hybrid model.

The current research focused on predicting the deflection of corroded reinforced concrete beams using numerical data collected from aging buildings, the integration of LSSVR with the seahorse optimizer has shown encouraging results. Although reducing the Kolmogorov complexity of the dataset is considered a potential way to improve model accuracy, prior studies [56, 57] have demonstrated that this method is typically more effective with complex datasets. Since the dataset in this study is standardized for specific technical applications, reducing its Kolmogorov complexity does not substantially improve the algorithm's performance. Therefore, the study concentrates on refining the algorithm and enhancing the model rather than altering the data structure.

4.4 Parametric analysis

To assess the contribution of each input parameter to the output parameter, a parametric analysis was conducted using the hybrid AI model. Leveraging the SHO-LSSVR model's potential, researchers conducted a comprehensive investigation to assess how different input parameter configurations influence the precision of deflection estimates for reinforced concrete beams undergoing corrosion. The research methodology systematically explored five distinct analytical scenarios, each probing unique subsets of the eight available parameters. The objective was to pinpoint the optimal configuration that would maximize predictive accuracy, with comprehensive results detailed in Table 4. The parameter selection process drew from an extensive foundation of previous scientific investigations and empirical evidence. Structural characteristics emerged as critical determinants in deflection prediction, with key factors including the reinforcement's cross-sectional area, rebar geometric properties, and the concrete's compressive strength proving particularly influential in modeling the complex

behavior of corroded reinforced concrete structural elements [29].

Table 4 comprehensively presents the performance outcomes from the training and testing phases across multiple analytical scenarios, with the third, fourth, and fifth experimental configurations demonstrating consistently promising results. Inputs such as X_8 (reinforcement area), X_7 (reinforcement diameter), and X_6 (concrete strength) drawing upon established research methodologies, these critical parameters have been substantiated as fundamental to precise deflection estimation in corroded reinforced concrete structures. The investigation underscores the paramount importance of strategic parameter selection and nuanced weighting techniques, demonstrating their pivotal role in improving the dependability and precision of computational models in structural engineering applications. For instance, presence or absence of a variable X_4 (protective concrete cover) has a notable effect on the accuracy of deflection predictions in reinforced concrete beams. The research tested various scenarios with differing input variables like beam dimensions, reinforcement area, and concrete strength, using the SHO-LSSVR model. Notably, omitting X_4 , which plays a critical role in preventing reinforcement corrosion and maintaining structural integrity, led to significant changes in prediction accuracy. This highlights the importance of protective concrete cover in accurately assessing structural performance.

<Insert Table 4 here>

To further evaluate the stability and applicability of the proposed SHO-LSSVR model, a parameter sensitivity analysis was conducted on the two key hyperparameters: kernel parameter (γ) and regularization parameter (C) . During the testing process, one parameter was varied while the other remained fixed at its optimal value. The first testing fold (fold 1) was selected for this analysis. Fig. 7 (a-b) illustrates the predictive outcomes for the initial data subset, demonstrating the impact of two critical tuning parameters on deflection estimation for corroded reinforced concrete beams. The analysis systematically examined these parameters across carefully defined intervals, spanning their established operational boundaries as identified through the SHO-LSSVR model's comprehensive five-fold assessment. For instance, Fig. 7a shows the prediction outcomes as the regularization parameter (C) varies. The findings suggest that the hybrid SHO-LSSVR model performs optimally when the (C) value is near 50, whereas deviations from this value lead to a decline in performance.

<Insert Fig. 7 here>

4.5 Discussion

By incorporating sophisticated machine learning methods, the SHO-LSSVR strategy shows enhanced predictive performance relative to conventional Support Vector Regression and

Artificial Neural Network techniques:

By integrating advanced machine learning techniques, the SHO-LSSVR approach demonstrates superior predictive capabilities compared to traditional Support Vector Regression and Artificial Neural Network methodologies. The research underscores how meticulous parameter optimization can significantly enhance model performance and accuracy. The innovative SHO-LSSVR approach distinguishes itself by employing a dynamic optimization strategy that transcends the limitations of conventional Support Vector Regression and Artificial Neural Network models. By leveraging SHO optimization techniques, the model can adaptively fine-tune parameters, ultimately delivering more precise and robust predictive capabilities.

The proposed ensemble prediction system outperforms individual ANN and SVM models by not only optimizing hyperparameters but also improving the overall efficiency of the integrated models. The hybrid architecture of the SHO-LSSVR model demonstrates a powerful synergy of advanced machine learning techniques, showcasing how integrated computational approaches can significantly enhance predictive accuracy and model robustness.

The accuracy of the testing folds is highly dependent on the model's ability to self-adjust its hyperparameters. Experimental findings reveal the critical challenges in hyperparameter selection for predictive models, particularly in complex structural engineering applications like assessing deflection in corroded reinforced concrete beams. The findings confirm that the SHO-LSSVR model is an effective instrument for planning structural management, providing improved prediction precision, dependability, and considerable savings in costs.

5 Conclusions

The research introduces an innovative multi-approach machine learning framework specifically tailored to forecast structural deformation in deteriorated reinforced concrete elements. Leveraging comprehensive empirical datasets, the proposed methodology outperforms conventional single-model and ensemble-based artificial intelligence techniques, offering a more nuanced and accurate predictive approach to structural analysis. The model's accuracy was evaluated using statistical metrics like root mean square error (RMSE), mean absolute error (MAE), mean absolute percentage error (MAPE), and R^2 , with results demonstrating that the hybrid seahorse optimizer and least squares support vector regression (SHO-LSSVR) model surpassed all competing models in forecasting deformation in deteriorated RC beams.

The SHO-LSSVR model utilizes LSSVR to model the relationship between deflection

01^ measurements and input variables, while the SHO refines the LSSVR hyperparameters to
 01^ improve accuracy. Researchers validated the predictive model using an extensive dataset
 02^ comprising 150 observations drawn from deteriorating residential structures located in southern
 02^ Vietnam. Through rigorous five-fold cross-validation, the methodology demonstrated
 02^ exceptional predictive capabilities. The performance metrics revealed impressive precision:
 02^ root mean square error of 1.896 mm, mean absolute error of 1.198 mm, mean absolute
 02^ percentage error of 0.547%, and a coefficient of determination of 0.891. These metrics
 02^ underscore the model's practical relevance in civil engineering and its potential adaptability to
 02^ tackle additional engineering challenges beyond deflection prediction in corroded RC beams.
 02^ This study aims to make a significant contribution to civil engineering by (i) proposing a
 02^ novel data-driven model that integrates machine learning with a nature-inspired metaheuristic
 02^ optimization method for widespread practical application, (ii) providing a comprehensive field
 03^ sample dataset to reliably evaluate the performance of ML models in forecasting deformation
 03^ in corroded RC beams, and (iii) offering civil engineers a valuable tool to address both current
 03^ and future challenges in the field.

03^ Acknowledgement

03^ We acknowledge Ho Chi Minh City University of Technology (HCMUT), VNU-HCM for
 03^ supporting this study.

03^ Appendix

03^ **Table A.** Details of 150 data

No	Surveyed Location	Location	X1	X2	X3	X4	X5	X6	X7	X8	Y
1	Block A of Da Lat market	7/X1o-X1 storey 1	6000.0	300.0	750.0	24.3	341.2	8.5	24.6	2454.4	9.099
2		X1'/1o-1 storey 1	6000.0	300.0	750.0	25.2	446.9	8.5	24.3	2454.4	11.972
3	Block B of Da Lat market	D'/9-9' storey 1	3500.0	200.0	400.0	23.4	94.9	11.5	19.6	1256.6	6.558
4		8/C'-D storey 1	3200.0	250.0	550.0	26.3	109.1	11.5	19.4	1963.5	2.029
5		F/9-9' storey 1	3500.0	250.0	550.0	27.5	126.2	11.5	19.8	1963.5	2.829
6		C'/9-9' storey 1	3500.0	200.0	400.0	28.3	77.0	11.5	19.7	1256.6	5.584
7		F'/9-9' storey 1	3500.0	200.0	400.0	24.7	59.4	11.5	19.3	1256.6	4.158
8	Asian International School - Cao Thang Campus	2/B-C storey 2	4800.0	250.0	500.0	28.1	71.2	13.0	24.2	9420.0	0.875
9		5/C-D storey 2	4780.0	250.0	500.0	27.2	71.2	13.0	24.1	9420.0	0.861
10	Lam Dong Ethnic Boarding School - Block A	8/D'-F storey 2	5900.0	200.0	550.0	25.5	111.8	11.5	19.4	1472.6	9.303
11		2/B-C storey 2	2990.0	200.0	300.0	24.6	4.1	8.5	15.2	628.3	0.802
12	274 Thong Nhat, Ward 16, Go Vap District	5/A-B storey 2	4960.0	100.0	300.0	24.8	2.0	8.5	15.7	402.0	1.736
13		2/C-D storey 2	3750.0	200.0	300.0	29.8	22.1	8.5	15.1	804.0	5.845
14		C/4-5 storey 2	3900.0	200.0	300.0	24.5	27.9	8.5	15.4	804.0	7.420
15		A/2-3 storey 2	3900.0	200.0	300.0	23.4	26.9	8.5	15.6	804.0	7.044

16		B34 storey 2	3900.0	200.0	300.0	20.8	21.2	8.5	15.8	804.0	5.353
17	Sports equipment-manufacturing factory.	4/A-B storey 1	6000.0	200.0	600.0	22.2	79.1	11.5	19.2	1112.0	7.011
18		6/A-B storey 1	4700.0	200.0	600.0	24.6	98.5	11.5	19.0	1391.0	4.464
19		3/A-B storey 1	4300.0	200.0	500.0	23.9	20.4	11.5	19.3	1005.0	1.554
20		3/A-B storey 1	4300.0	200.0	500.0	25.8	51.4	11.5	19.5	1392.0	2.978
21	Coop Mart Binh Tan	2/K-G storey 4	6000.0	250.0	550.0	26.2	188.7	8.5	19.5	1885.0	13.206
22		2/G-E storey 4	6000.0	250.0	550.0	25.3	103.0	8.5	19.7	1885.0	7.161
23		2/E-C storey 4	6000.0	250.0	550.0	24.2	102.5	8.5	19.6	1885.0	7.069
24		2/C-A storey 4	6000.0	250.0	550.0	23.6	191.9	8.5	19.4	1885.0	13.183
25		9/K-G storey 4	6000.0	250.0	550.0	22.7	138.2	8.5	19.3	1885.0	9.437
26		9/G-E storey 4	6000.0	250.0	550.0	26.1	105.5	8.5	19.3	1885.0	7.376
27		9/E-C storey 4	6000.0	250.0	550.0	28.4	103.9	8.5	19.8	1885.0	7.383
28		9/C-A storey 4	6000.0	250.0	550.0	22.4	112.9	8.5	19.7	1885.0	7.694
29		E/1o-1 storey 4	6000.0	200.0	450.0	25.3	29.0	8.5	19.4	1345.0	4.404
30		E/1-11 storey 4	4500.0	200.0	300.0	23.4	22.1	8.5	15.4	804.0	7.648
31	118 Ban Co, Ward 3, District 3, HCMC	B/5-6 storey 2	3000.0	150.0	300.0	21.2	18.4	8.5	15.2	427.0	4.989
32		B/5-6 storey 2	3000.0	200.0	300.0	23.4	14.1	8.5	15.7	508.9	3.249
33		6/A-B storey 2	3000.0	200.0	250.0	22.5	17.7	8.5	15.2	427.3	7.300
34		6/B'-C storey 2	3200.0	200.0	300.0	24.5	24.0	8.5	15.6	508.9	6.378
35	148 Ly Chinh Thang, District 3, HCMC	3/A-B storey 2	3200.0	200.0	300.0	23.4	46.2	8.5	15.8	508.9	12.092
36		B/4-5 storey 1	3200.0	200.0	300.0	22.4	13.9	8.5	15.4	402.1	4.411
37		4/A-C storey 2	3500.0	200.0	300.0	26.8	28.4	8.5	15.2	508.9	9.301
38	Psychiatric hospital in Ho Chi Minh city	10/D-E storey 3	5000.0	400.0	450.0	23.7	151.0	14.5	24.6	2777.0	7.221
39		2/F-G storey 2	5000.0	400.0	450.0	22.4	162.8	14.5	24.4	2280.0	9.159
40		E/10-11 storey 1	5500.0	400.0	450.0	24.1	115.8	14.5	24.1	2513.0	7.334
41		G/1-2 storey 2	5500.0	400.0	450.0	26.2	151.1	14.5	24.9	2513.0	9.737
42	67 Street 9, Quarter 2, Linh Tay Ward, HCMC	B/2-3 storey 2	3000.0	200.0	400.0	24.6	41.7	11.5	15.2	804.0	3.152
43	291 Street 7, Binh Tri Dong Ward, HCMC	3/A-C storey 2	3000.0	200.0	300.0	24.4	26.9	8.5	19.7	1005.0	3.443
44	2 Quarter 3, Phu My Ward, HCMC	1/D-A storey 2	5000.0	400.0	400.0	23.8	117.5	11.5	24.8	2513.0	8.279
45		5/A-B storey 2	5000.0	200.0	400.0	22.8	42.8	11.5	19.1	804.0	8.837
46	Southern Electricity, HCMC	6a/Ca-Ea storey 2	5000.0	250.0	900.0	26.7	116.2	8.5	19.6	3928.0	0.961
47		6a/Ca-storey 3	5000.0	250.0	900.0	24.2	111.9	8.5	19.5	3928.0	0.916
48	106 D3 Street, Binh Thanh District, HCMC	A/1-2 storey 4	4200.0	200.0	300.0	23.2	4.8	8.5	15.2	603.0	1.847
49		A/1-2 storey 2	4200.0	200.0	300.0	21.5	20.6	8.5	15.4	603.0	7.828
50		B/1-2 storey 2	4200.0	200.0	500.0	22.8	18.3	8.5	15.2	603.0	2.130
51		C/1-2 storey 4	4200.0	200.0	300.0	26.8	30.4	8.5	15.4	603.0	12.342
52		F/1-2 storey 1	4200.0	200.0	300.0	24.1	30.5	8.5	15.7	603.0	11.966
53	corridor at Tan Son Nhat airport	20/K3-K4 storey 1	3700.0	1200.0	250.0	22.8	91.8	11.5	19.3	2001.0	11.392
54		19'-20/N storey 1	3700.0	250.0	350.0	26.4	46.7	11.5	19.6	1017.0	5.953
55		19'-20/G20 storey 1	3500.0	250.0	350.0	22.5	72.8	11.5	19.5	1017.0	7.960

56	Head office of aquatic feed factory, Lo Vap district, Dong Thap province	4/A-A' storey 1	5200.0	300.0	500.0	21.9	50.1	13.0	19.1	942.0	5.407
57		4/B-C storey 1	5200.0	600.0	500.0	20.7	132.8	13.0	19.4	1257.0	10.085
58		4/A-B storey 3	3700.0	300.0	500.0	20.4	100.6	13.0	19.6	942.0	5.441
59		4/C-D storey 3	3700.0	300.0	500.0	24.1	94.5	13.0	19.4	942.0	5.238
60		4/C-D storey 4	5250.0	300.0	500.0	28.4	60.6	13.0	19.2	942.0	6.954
61		4/A-B storey 5	3750.0	300.0	500.0	27.1	116.1	13.0	19.3	1257.0	5.260
62		4/C-D storey 6	5200.0	300.0	500.0	26.8	155.1	13.0	19.4	1257.0	13.485
63		4/B-C storey 7	5200.0	300.0	500.0	25.0	102.2	13.0	19.8	1257.0	8.779
64		4/B-C storey 8	3750.0	500.0	500.0	23.3	125.1	13.0	19.9	1473.0	4.493
65		4/C-D storey 8	5250.0	300.0	500.0	24.8	121.7	13.0	19.3	1659.0	8.357
66		4/A-B storey 9	3750.0	500.0	500.0	26.4	52.5	13.0	19.4	1232.0	2.241
67		4/C-D storey 9	5250.0	300.0	500.0	25.3	46.2	13.0	19.7	829.0	5.800
68		4/A-B storey 10	3800.0	400.0	500.0	24.1	58.4	13.0	19.5	1659.0	2.013
69		4/C-D storey 10	1800.0	400.0	500.0	28.6	402.6	13.0	19.4	1659.0	3.213
70	b195 storey 11	3800.0	300.0	500.0	26.2	57.1	13.0	19.3	628.0	4.792	
71	4/C-D storey 12	4800.0	300.0	500.0	25.1	42.3	13.0	19.3	1030.0	3.675	
72	B axle frame	B/3-4 storey 1	6200.0	300.0	500.0	29.4	59.6	13.0	19.4	1030.0	8.902
73		B/3-4 storey 2	6200.0	300.0	500.0	25.1	61.9	13.0	19.3	1030.0	8.981
74		B/1-2 storey 2	6200.0	300.0	500.0	26.5	63.5	13.0	19.2	1030.0	9.293
75		B/1-2 storey 3	6600.0	300.0	500.0	25.3	69.5	13.0	19.8	1030.0	11.434
76		B/2-3 storey 4	4800.0	300.0	500.0	23.4	125.9	13.0	19.5	2061.0	5.913
77		B/1-2 storey 4	6200.0	300.0	500.0	26.1	78.1	13.0	19.3	1030.0	11.403
78		B/3-4 storey 5	6250.0	300.0	500.0	23.4	72.1	13.0	19.6	1030.0	10.510
79		B/1-2 storey 6	6650.0	300.0	500.0	28.1	68.7	13.0	19.1	1030.0	11.699
80		B/2-3 storey 13	4950.0	200.0	400.0	26.1	26.9	13.0	15.2	402.0	9.999
81		B/2-3 storey 12	4950.0	200.0	400.0	24.6	13.3	13.0	15.8	402.0	4.893
82		b102 storey 11	1500.0	300.0	500.0	24.8	216.3	13.0	19.6	942.0	1.980
83		b92 storey 12	1850.0	200.0	400.0	24.8	42.6	13.0	15.2	804.0	1.210
84	C axle frame	A/2-3 storey 2	5100.0	300.0	600.0	23.4	8.2	13.0	15.1	603.0	0.833
85		A/3-4 storey 2	6500.0	600.0	600.0	22.8	69.5	13.0	15.4	603.0	10.483
86		2/A-A' storey 3	3700.0	600.0	600.0	23.4	331.5	13.0	19.9	4398.0	2.887
87		b27 storey 3	3000.0	600.0	600.0	22.3	339.2	13.0	19.7	4398.0	1.929
88		2/A-A' storey 4	3700.0	600.0	600.0	20.8	502.8	13.0	19.2	3770.0	4.938
89		1/A-A' storey 8	2750.0	500.0	600.0	23.6	458.5	13.0	24.1	4025.0	2.440
90		2/A-A' storey 8	2750.0	500.0	600.0	24.2	491.6	13.0	24.5	4025.0	2.625
91		3/A-A' storey 8	2750.0	500.0	600.0	23.6	496.4	13.0	24.8	4025.0	2.641
92		3/A-A' storey 8	3000.0	200.0	500.0	28.1	84.7	13.0	15.2	402.0	6.968
93		C/5-5' storey 8	3000.0	200.0	500.0	24.6	70.9	13.0	15.2	804.0	3.141
94		b23 storey 9	2750.0	500.0	500.0	25.8	194.4	13.0	24.2	4025.0	1.591
95		b25 storey 9	2750.0	500.0	500.0	26.4	249.6	13.0	24.9	4025.0	2.052
96		b27 storey 9	2750.0	500.0	500.0	28.2	248.0	13.0	24.6	4025.0	2.067
97		b29 storey 9	3000.0	200.0	500.0	23.7	46.8	13.0	15.8	402.0	3.745
98		b55 storey 9	1750.0	500.0	500.0	26.2	89.9	13.0	24.8	2576.0	0.442
99	b156 storey 9	3000.0	200.0	500.0	24.8	56.0	13.0	15.3	804.0	2.484	

100		b187 storey 9	3000.0	500.0	600.0	24.7	188.1	13.0	24.2	3142.0	1.490
101		b126 storey 9	3000.0	500.0	600.0	21.2	215.6	13.0	24.3	4025.0	1.346
102		b196 storey 10	1800.0	200.0	500.0	24.9	21.3	13.0	15.8	603.0	0.435
103		b196 storey 11	1800.0	200.0	500.0	23.1	18.6	13.0	15.3	603.0	0.377
104		b103 storey12	2000.0	200.0	400.0	21.6	45.6	13.0	15.7	804.0	1.468
105		B/2-3 storey 6	4800.0	300.0	500.0	24.3	121.8	13.0	19.1	804.0	13.042
106		B/1-2 storey 6	6200.0	300.0	500.0	28.1	75.1	13.0	19.9	1030.0	11.111
107		b102 storey 6	1500.0	300.0	500.0	25.4	93.6	13.0	19.7	1659.0	0.527
108		b102 storey 5	1500.0	300.0	500.0	28.2	95.7	13.0	19.3	1659.0	0.550
109		B/2-3 storey 2	4800.0	300.0	500.0	26.7	123.8	13.0	19.5	1659.0	7.204
110		B/1-2 storey 1	6200.0	300.0	500.0	32.6	64.9	13.0	19.8	1030.0	9.912
111		B/2-3 storey 3	4800.0	300.0	500.0	30.4	125.3	13.0	19.6	1659.0	7.488
112		4/C-D storey 1	3700.0	300.0	500.0	31.5	97.6	13.0	19.9	1546.0	3.715
113		4/B-C storey 2	5200.0	300.0	500.0	24.8	127.8	13.0	19.7	1659.0	8.611
114		4/C-D storey 2	3700.0	300.0	500.0	27.6	125.0	13.0	19.8	1345.0	5.219
115		4/A-B storey 3	5200.0	600.0	500.0	24.8	278.9	13.0	24.2	2878.0	10.633
116		4/A-B storey 4	3700.0	600.0	600.0	20.7	574.3	13.0	24.7	4398.0	4.922
117		4/B-C storey 5	5200.0	300.0	500.0	23.8	109.2	13.0	19.8	1257.0	9.298
118		4/B-C storey 4	5200.0	300.0	500.0	24.6	126.0	13.0	19.1	1659.0	8.477
119		4/A-B storey 6	5250.0	300.0	500.0	21.8	138.9	13.0	19.8	1257.0	11.892
120		b165 storey 7	3750.0	300.0	500.0	24.8	86.8	13.0	19.6	1257.0	3.872
121		b18 storey 3	3700.0	600.0	600.0	26.3	318.1	13.0	24.6	4398.0	2.818
122		4/B-C storey 9	5200.0	300.0	500.0	27.1	52.5	13.0	19.7	1232.0	4.650
123		b123 storey 10	5200.0	300.0	500.0	26.4	80.8	13.0	19.6	942.0	8.981
124		4/C-D storey 11	3800.0	400.0	500.0	23.6	38.1	13.0	19.6	1659.0	1.311
125		4/C-D storey 12	3800.0	300.0	500.0	28.1	14.1	13.0	15.3	628.0	1.194
126		b102 storey 3	6200.0	300.0	500.0	20.4	143.1	13.0	19.8	1659.0	13.279
127		B/2-3 storey 5	4800.0	300.0	500.0	28.2	126.0	13.0	19.2	2061.0	6.130
128		B/1-2 storey 7	4800.0	300.0	500.0	22.7	119.4	13.0	19.6	2061.0	5.578
129		B/3-4 storey 8	6250.0	300.0	500.0	21.3	114.1	13.0	19.5	1659.0	10.834
130		B/1-2 storey 8	6200.0	300.0	500.0	26.1	137.8	13.0	19.4	1659.0	13.321
131		B/2-3 storey 9	4800.0	300.0	500.0	21.9	106.7	13.0	19.7	1659.0	6.002
132		B/1-2 storey 9	6200.0	300.0	500.0	24.3	129.8	13.0	19.3	1659.0	12.387
133		B/2-3 storey 10	4800.0	300.0	500.0	28.3	101.2	13.0	19.8	1257.0	7.573
134	Dong Thap office building	4/B-C storey 4	5200.0	300.0	500.0	24.3	126.0	13.0	19.3	1659.0	8.459
135		4/C-D storey 4	3700.0	300.0	500.0	24.6	111.7	13.0	19.5	1659.0	3.805
136		4/A-B storey 5	5250.0	300.0	500.0	25.3	142.6	13.0	19.6	1257.0	12.504
137		4/B-C storey 5	5200.0	300.0	500.0	22.4	124.6	13.0	19.2	1257.0	10.508
138		4/C-D storey 5	3750.0	300.0	500.0	21.6	113.3	13.0	19.7	1257.0	4.944
139		4/B-C storey 6	3670.0	300.0	500.0	24.1	66.1	13.0	19.2	942.0	3.606
140		4/A-B storey 8	5250.0	300.0	500.0	28.2	128.7	13.0	19.3	1659.0	9.052
141		4/B-C storey 8	5200.0	300.0	500.0	23.4	102.2	13.0	19.5	942.0	11.143
142		4/C-D storey 9	3750.0	500.0	500.0	23.8	107.2	13.0	24.6	4025.0	1.607
143			b215 storey 9	3000.0	500.0	500.0	24.2	192.7	13.0	24.3	4025.0

144		4/C-D storey 10	3800.0	400.0	500.0	26.4	58.4	13.0	19.4	1659.0	2.045
145		b165 storey 11	3800.0	300.0	500.0	23.5	14.1	13.0	15.5	628.0	1.160
146	Vocational School No. 12 Quang Trung, Go Vap District, HCMC	b14 storey 2	4200.0	200.0	500.0	24.7	18.8	8.5	15.2	603.0	2.213
147		b20 storey 4	4200.0	200.0	300.0	26.1	30.4	8.5	15.3	603.0	12.266
148		b20 storey 1	4200.0	200.0	500.0	20.8	24.4	8.5	15.0	603.0	2.800
149		b23 storey 3	4200.0	200.0	500.0	24.8	15.4	8.5	15.7	603.0	1.817
150		b23 storey 1	4200.0	200.0	500.0	26.5	20.7	8.5	15.4	603.0	2.477

038

0396 References

- 040[1] Thirumalaiselvi, A. and Sasmal, S. "Machine learning-based acoustic emission
041 technique for corrosion-induced damage monitoring in reinforced concrete structures",
042 *Engineering Applications of Artificial Intelligence*, **137**, p. 109121.
043 <https://doi.org/10.1016/j.engappai.2024.109121> (2024).
- 044[2] Xi, X., Yin, Z., Yang, S. *et al.* "Machine learning-based reliability analysis of structural
045 concrete cracking considering realistic nonuniform corrosion development", *Journal of*
046 *Structural Engineering*, **150**(1), p. 04023207. <https://doi.org/10.1061/jsendh.steng-12253>
047 (2024).
- 048[3] Huang, T., Wan, C., Liu, T. *et al.* "Degradation law of bond strength of reinforced
049 concrete with corrosion-induced cracks and machine learning prediction model", *Journal of*
050 *Building Engineering*, **98**, p. 111022. <https://doi.org/10.1016/j.jobe.2024.111022> (2024).
- 051[4] Fernandez, I., Herrador, M. F., Marí, A. R. *et al.* "Structural effects of steel
052 reinforcement corrosion on statically indeterminate reinforced concrete members", *Materials*
053 *and Structures*, **49**(12), pp. 4959-4973. <https://doi.org/10.1617/s11527-016-0836-2> (2016).
- 054[5] Aydin, A., Bilen, M., and Maali, M. "Effect of hydrochloric acid corrosion and CFRP
055 coating on the buckling behavior of cylindrical shells under external pressure", *Scientia*
056 *Iranica*, **29**(6), pp. 2886-2901. <https://doi.org/10.24200/sci.2021.57618.5332> (2022).
- 057[6] Shayanfar, M. A., Hatami, A., Zabihi-Samani, M. *et al.* "Simulation of the force-
058 displacement behavior of reinforced concrete beams under different degrees and locations of
059 corrosion", *Scientia Iranica*, **29**(3), pp. 964-972.
060 <https://doi.org/10.24200/sci.2021.55422.4214> (2022).
- 061[7] Hu, J., Zhang, S., Chen, E. *et al.* "A review on corrosion detection and protection of
062 existing reinforced concrete (RC) structures", *Construction and Building Materials*, **325**, p.
063 126718. <https://doi.org/10.1016/j.conbuildmat.2022.126718> (2022).
- 064[8] Fahimi, S., Zakerzadeh, M., Baghani, M. *et al.* "A novel method for implementation of
065 corrosion-induced cracks in the finite element models of reinforced concrete structures",
066 *Scientia Iranica*, **28**(3), pp. 1079-1095. [10.24200/sci.2020.52829.2903](https://doi.org/10.24200/sci.2020.52829.2903) (2021).
- 067[9] Rodrigues, R., Gaboreau, S., Gance, J. *et al.* "Reinforced concrete structures: A review
068 of corrosion mechanisms and advances in electrical methods for corrosion monitoring",
069 *Construction and Building Materials*, **269**, p. 121240.
070 <https://doi.org/10.1016/j.conbuildmat.2020.121240> (2021).
- 071[10] Nguyen, T.-H., Tran, D.-H., Nguyen, N.-M. *et al.* "Accurately predicting the
072 mechanical behavior of deteriorated reinforced concrete components using natural
073 intelligence-integrated Machine learners", *Construction and Building Materials*, **408**, p.
074 133753. <https://doi.org/10.1016/j.conbuildmat.2023.133753> (2023).
- 075[11] Bai, C., Nguyen, H., Asteris, P. G. *et al.* "A refreshing view of soft computing models
076 for predicting the deflection of reinforced concrete beams", *Applied Soft Computing*, **97**, p.
077 106831. <https://doi.org/10.1016/j.asoc.2020.106831> (2020).

- 058[12] Song, L., Fan, Z., and Hou, J. "Experimental and analytical investigation of the fatigue
059 flexural behavior of corroded reinforced concrete beams", *International Journal of Concrete*
080 *Structures and Materials*, **13**, pp. 1-14. <https://doi.org/10.1186/s40069-019-0340-5> (2019).
- 081[13] Matthews, B., Palermo, A., Logan, T. *et al.* "Experimental testing and predictive
082 machine learning to determine the mechanical characteristics of corroded reinforcing steel",
083 *Construction and Building Materials*, **438**, p. 137023.
084 <https://doi.org/10.1016/j.conbuildmat.2024.137023> (2024).
- 085[14] Al-Huri, M. A., Al-Osta, M. A., and Ahmad, S. "Finite element modelling of corrosion-
086 damaged RC beams strengthened using the UHPC layers", *Materials*, **15**(21), p. 7606.
087 <https://doi.org/10.3390/ma15217606> (2022).
- 088[15] Nguyen, T.-H., Nguyen, D.-T., Nguyen, D.-H. *et al.* "Evaluation of residual strength of
089 corroded reinforced concrete beams using machine learning models", *Arabian Journal for*
090 *Science and Engineering*, **47**(8), pp. 9985-10002. [https://doi.org/10.1007/s13369-021-06493-](https://doi.org/10.1007/s13369-021-06493-8)
091 [8](https://doi.org/10.1007/s13369-021-06493-8) (2022).
- 092[16] Meda, A., Mostosi, S., Rinaldi, Z. *et al.* "Experimental evaluation of the corrosion
093 influence on the cyclic behaviour of RC columns", *Engineering Structures*, **76**, pp. 112-123.
094 <https://doi.org/10.1016/j.engstruct.2014.06.043> (2014).
- 095[17] Ojha, S. and Shelke, A. "Estimation of the Remaining Useful Life of Axially Loaded
096 Members Through Nested Least-Square Support Vector Regression", *Journal of Earthquake*
097 *Engineering*, **29**(1), pp. 243-264. <https://doi.org/10.1080/13632469.2024.2424176> (2025).
- 098[18] Nassif, N., Talha Junaid, M., Hamad, K. *et al.* "Performance-based prediction of shear
099 and flexural strengths in fiber-reinforced concrete beams via machine learning", *Structural*
100 *Engineering International*, **34**(4), pp. 651-656.
101 <https://doi.org/10.1080/10168664.2024.2310520> (2024).
- 102[19] Emami, F. and Kabir, M. Z. "Strength prediction of composite metal deck slabs under
103 free drop weight impact loading using numerical approach and data set machine learning",
104 *Scientia Iranica*, <https://doi.org/10.24200/sci.2023.59582.6321> (2023).
- 105[20] Sharma, A., Sharma, S., and Kumar, K., "A machine learning based model to assess
106 flexural strength of corroded reinforced concrete beams", *International Conference on*
107 *Structural Engineering and Construction Management*: Springer
108 https://doi.org/10.1007/978-3-031-39663-2_81 (2023).
- 109[21] Amezquita-Sancheza, J., Valtierra-Rodriguez, M., and Adeli, H. "Machine learning in
110 structural engineering", *Scientia Iranica*, **27**(6), pp. 2645-2656. [10.24200/sci.2020.22091](https://doi.org/10.24200/sci.2020.22091)
111 (2020).
- 112[22] Güleriyüz, D., Efe, Ö. F., and Efe, B. "Estimation of Anthropometric Measurements
113 Using Optimized Machine Learning Models with Bayesian Algorithm", *Scientia Iranica*,
114 <https://doi.org/10.24200/sci.2023.61224.7209> (2023).
- 115[23] Suykens, J. A., Van Gestel, T., De Brabanter, J. *et al.*, *Least squares support vector*
116 *machines*. World scientific. <https://doi.org/10.1142/9789812776655> (2002).
- 117[24] Safonova, A., Ghazaryan, G., Stiller, S. *et al.* "Ten deep learning techniques to address
118 small data problems with remote sensing", *International Journal of Applied Earth*
119 *Observation and Geoinformation*, **125**, p. 103569. <https://doi.org/10.1016/j.jag.2023.103569>
120 (2023).
- 121[25] Zhao, S., Zhang, T., Ma, S. *et al.* "Sea-horse optimizer: a novel nature-inspired meta-
122 heuristic for global optimization problems", *Applied Intelligence*, **53**(10), pp. 11833-11860.
123 <https://doi.org/10.1007/s10489-022-03994-3> (2023).
- 124[26] Nguyen, N.-T., Tran, Q., Dao, C.-H. *et al.* "Automatic detection of personal protective
125 equipment in construction sites using metaheuristic optimized YOLOv5", *Arabian Journal*
126 *for Science and Engineering*, **49**(10), pp. 13519-13537. [https://doi.org/10.1007/s13369-023-](https://doi.org/10.1007/s13369-023-08700-0)
127 [08700-0](https://doi.org/10.1007/s13369-023-08700-0) (2024).

- 728[27] Pham, A.-D., Ngo, N.-T., and Nguyen, T.-K. "Machine learning for predicting long-
729 term deflections in reinforce concrete flexural structures", *Journal of Computational Design*
730 *and Engineering*, **7**(1), pp. 95-106. <https://doi.org/10.1093/jcde/qwaa010> (2020).
- 731[28] Li, N., Asteris, P. G., Tran, T.-T. *et al.* "Modelling the deflection of reinforced concrete
732 beams using the improved artificial neural network by imperialist competitive optimization",
733 *Steel and Composite Structures, An International Journal*, **42**(6), pp. 733-745.
734 <https://doi.org/10.12989/scs.2022.42.6.733> (2022).
- 735[29] Nguyen, N.-M., Wang, W.-C., and Cao, M.-T. "Early estimation of the long-term
736 deflection of reinforced concrete beams using surrogate models", *Construction and Building*
737 *Materials*, **370**, p. 130670. <https://doi.org/10.1016/j.conbuildmat.2023.130670> (2023).
- 738[30] TCVN "Heavy weight concrete - Method for determination of compressive strength by
739 rebound hammer", <https://moc.gov.vn/en/Pages/default.aspx> (2012).
- 740[31] TCVN "Normal concrete - Nondestructive methods - Assessment of concrete quality
741 using ultrasonic pulse velocity", <https://moc.gov.vn/en/Pages/default.aspx> (2012).
- 742[32] TCVN "Fresh and hardened concrete - Sampling, making and curing of test specimens",
743 <https://moc.gov.vn/en/Pages/default.aspx> (2022).
- 744[33] Kim, S.-W. and Kim, K.-H. "Prediction of deflection of reinforced concrete beams
745 considering shear effect", *Materials*, **14**(21), p. 6684. <https://doi.org/10.3390/ma14216684>
746 (2021).
- 747[34] Gribniak, V., Cervenka, V., and Kaklauskas, G. "Deflection prediction of reinforced
748 concrete beams by design codes and computer simulation", *Engineering Structures*, **56**, pp.
749 2175-2186. <https://doi.org/10.1016/j.engstruct.2013.08.045> (2013).
- 750[35] Cheng, M.-Y. and Cao, M.-T. "Evolutionary multivariate adaptive regression splines
751 for estimating shear strength in reinforced-concrete deep beams", *Engineering Applications*
752 *of Artificial Intelligence*, **28**, pp. 86-96. <https://doi.org/10.1016/j.engappai.2013.11.001>
753 (2014).
- 754[36] Kaczmarek, M. and Szymańska, A. "Application of artificial neural networks to predict
755 the deflections of reinforced concrete beams", *Studia Geotechnica et Mechanica*, **38**(2),
756 <https://doi.org/10.1515/sgem-2016-0017> (2016).
- 757[37] Mohammadhassani, M., Nezamabadi-Pour, H., Jumaat, M. Z. *et al.* "Application of
758 artificial neural networks (ANNs) and linear regressions (LR) to predict the deflection of
759 concrete deep beams", *Computers and Concrete*, **11**(3), pp. 237-252.
760 <https://doi.org/10.12989/cac.2013.11.3.237> (2013).
- 761[38] Mishra, M., Agarwal, A., and Maity, D. "Neural-network-based approach to predict the
762 deflection of plain, steel-reinforced, and bamboo-reinforced concrete beams from
763 experimental data", *SN Applied Sciences*, **1**, pp. 1-11. <https://doi.org/10.1007/s42452-019-0622-1>
764 (2019).
- 765[39] Nguyen, H. D., Zhang, Q., Choi, E. *et al.* "An improved deflection model for FRP RC
766 beams using an artificial intelligence-based approach", *Engineering structures*, **219**, p.
767 110793. <https://doi.org/10.1016/j.engstruct.2020.110793> (2020).
- 768[40] Vijayan, D. "Prediction of displacement in Reinforced concrete based on artificial
769 neural networks using sensors", *Measurement: Sensors*, **27**, p. 100764.
770 <https://doi.org/10.1016/j.measen.2023.100764> (2023).
- 771[41] Inc, S., "PASW statistics for Windows," ed: SPSS Inc. Chicago,
772 <http://www.spss.com.hk/statistics/> (2009).
- 773[42] Mathworks, I. "MATLAB and statistics toolbox release 2012b", *Natick (Massachusetts,*
774 *United States)*, https://www.mathworks.com/?s_tid=gn_logo (2012).
- 775[43] Faghihi Nezhad, M. and Minaei Bidgoli, B. "Development of an ensemble learning-
776 based intelligent model for stock market forecasting", *Scientia Iranica*, **28**(1), pp. 395-411.
777 <https://doi.org/10.24200/sci.2019.50353.1654> (2021).

- 778[44] Drobiec, Ł., Jasiński, R., and Mazur, W. "Accuracy of eddy-current and radar methods
779 used in reinforcement detection", *Materials*, **12**(7), p. 1168.
780 <https://doi.org/10.3390/ma12071168> (2019).
- 781[45] Donkervoort, J. "Reuse of concrete elements", *Masters graduation thesis, Eindhoven
782 University of Technology, Eindhoven, Netherlands*,
783 <https://research.tue.nl/en/studentHeres/reuse-of-concrete-elements> (2024).
- 784[46] TCVN "Fresh and hardened concrete – Sampling, making and curing of test specimens",
785 <https://moc.gov.vn/en/Pages/default.aspx> (2002).
- 786[47] TCVN "Concrete - Ultrasonic method for defect detection",
787 <https://moc.gov.vn/en/Pages/default.aspx> (2022).
- 788[48] TCVN "Heavyweight concrete – Guide to assessment of concrete strength in existing
789 structures", <https://moc.gov.vn/en/Pages/default.aspx> (2006).
- 790[49] TCVN "Hardened concrete - Test method for compressive strength",
791 <https://moc.gov.vn/en/Pages/default.aspx> (2022).
- 792[50] TCVN "Reinforced concrete structures - Electromagnetic method for determining
793 thickness of concrete-cover and location and diameter of steel bar in the concrete",
794 <https://moc.gov.vn/en/Pages/default.aspx> (2012).
- 795[51] TCVN "Design of concrete and reinforced concrete structures",
796 <https://moc.gov.vn/en/Pages/default.aspx> (2018).
- 797[52] Chou, J.-S. and Pham, A.-D. "Enhanced artificial intelligence for ensemble approach to
798 predicting high performance concrete compressive strength", *Construction and Building
799 Materials*, **49**, pp. 554-563. <https://doi.org/10.1016/j.conbuildmat.2013.08.078> (2013).
- 800[53] Chou, J.-S. and Bui, D.-K. "Modeling heating and cooling loads by artificial intelligence
801 for energy-efficient building design", *Energy and Buildings*, **82**, pp. 437-446.
802 <https://doi.org/10.1016/j.enbuild.2014.07.036> (2014).
- 803[54] Prayogo, D., Cheng, M.-Y., Wu, Y.-W. *et al.* "Combining machine learning models via
804 adaptive ensemble weighting for prediction of shear capacity of reinforced-concrete deep
805 beams", *Engineering with Computers*, **36**(3), pp. 1135-1153. [https://doi.org/10.1007/s00366-
806 019-00753-w](https://doi.org/10.1007/s00366-019-00753-w) (2020).
- 807[55] Bishop, C. M. and Nasrabadi, N. M., *Pattern recognition and machine learning* (no. 4).
808 Springer. <https://doi.org/10.1007/978-1-4615-7566-5> (2006).
- 809[56] Kabir, H. and Garg, N. "Machine learning enabled orthogonal camera goniometry for
810 accurate and robust contact angle measurements", *Scientific reports*, **13**(1), p. 1497.
811 <https://doi.org/10.1038/s41598-023-28763-1> (2023).
- 812[57] Bolón-Canedo, V. and Remeseiro, B. "Feature selection in image analysis: a survey",
813 *Artificial Intelligence Review*, **53**(4), pp. 2905-2931. [https://doi.org/10.1007/s10462-019-
814 09750-3](https://doi.org/10.1007/s10462-019-09750-3) (2020).
- 815

List of figures

۷۱۷ Fig. 1. Flow chart of hybrid SHO-LSSVR model..... 25

۷۱۸ Fig. 2. Evaluation of concrete cracks and the visibility of reinforced concrete beams. ... 26

۷۱۹ Fig. 3. Assessing concrete strength and measuring reinforcement diameter 26

۷۲۰ Fig. 4. Modelling stream for predicting deflection in corroded RC beams. 27

۷۲۱ Fig. 5. Visualization of average performance results for the predictive models..... 27

۷۲۲ Fig. 6. Absolute deviation for the best testing fold of all models 27

۷۲۳ Fig. 7. Influence of model input parameters 28

۷۲۴

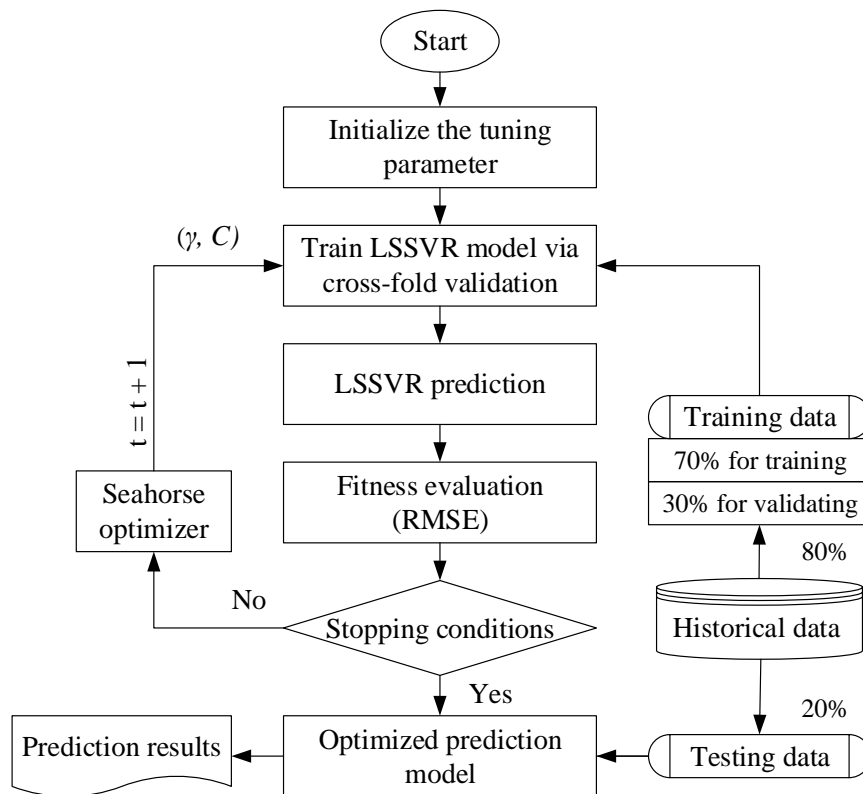
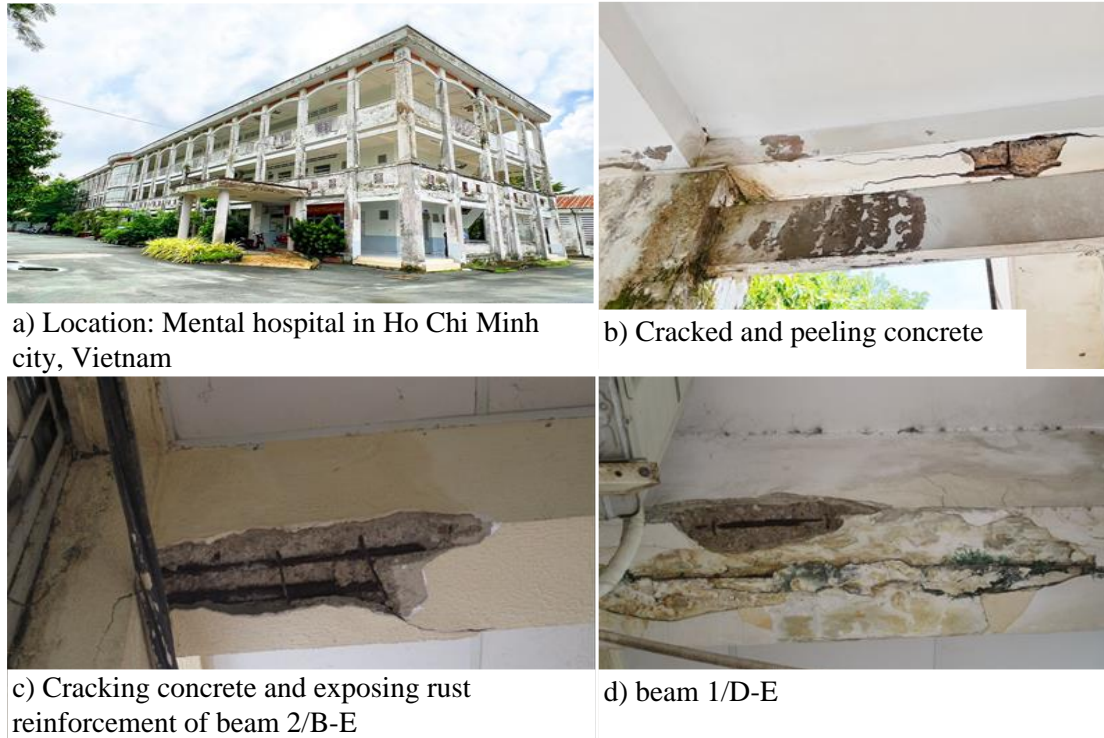
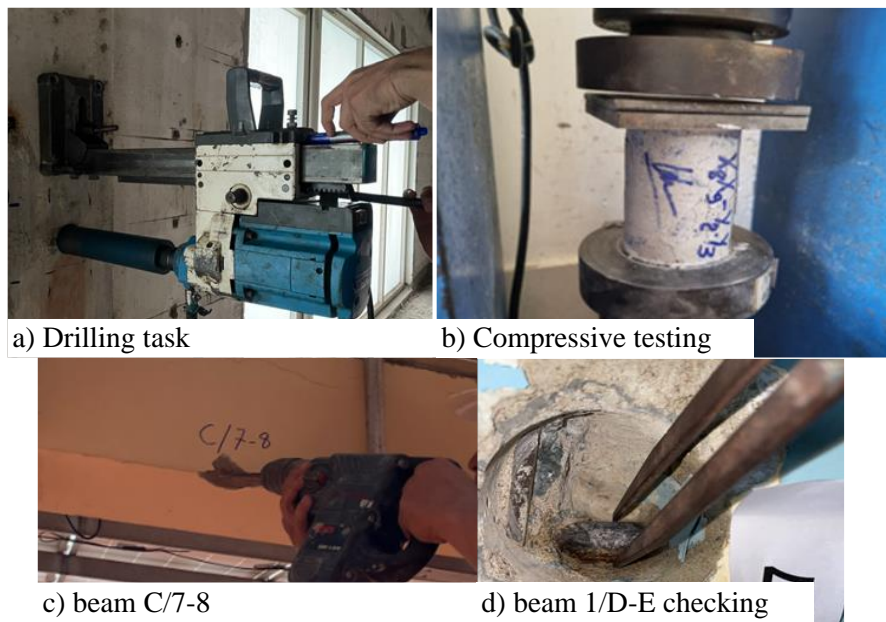


Fig. 1. Flow chart of hybrid SHO-LSSVR model.



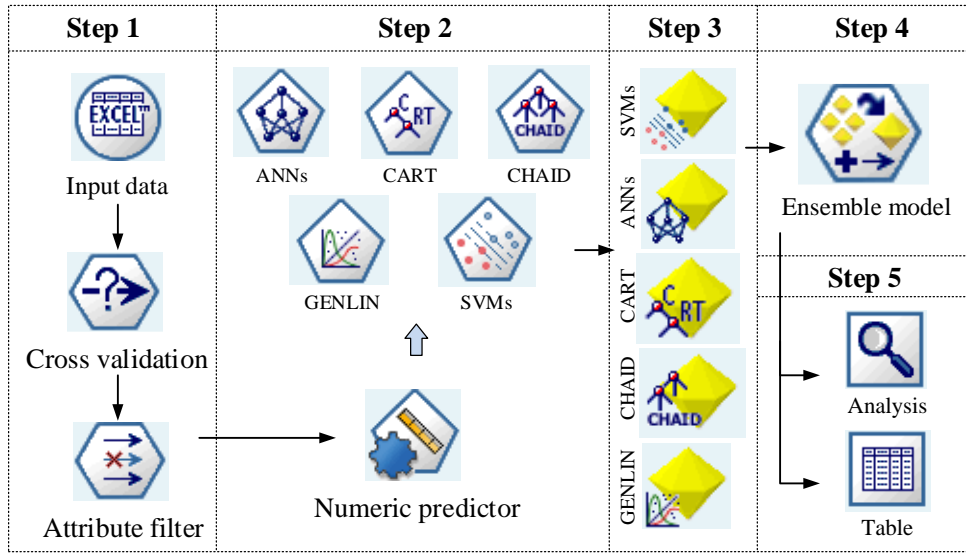
۷۲۸
۷۲۹
۷۳۰
۷۳۱

Fig. 2. Evaluation of concrete cracks and the visibility of reinforced concrete beams.



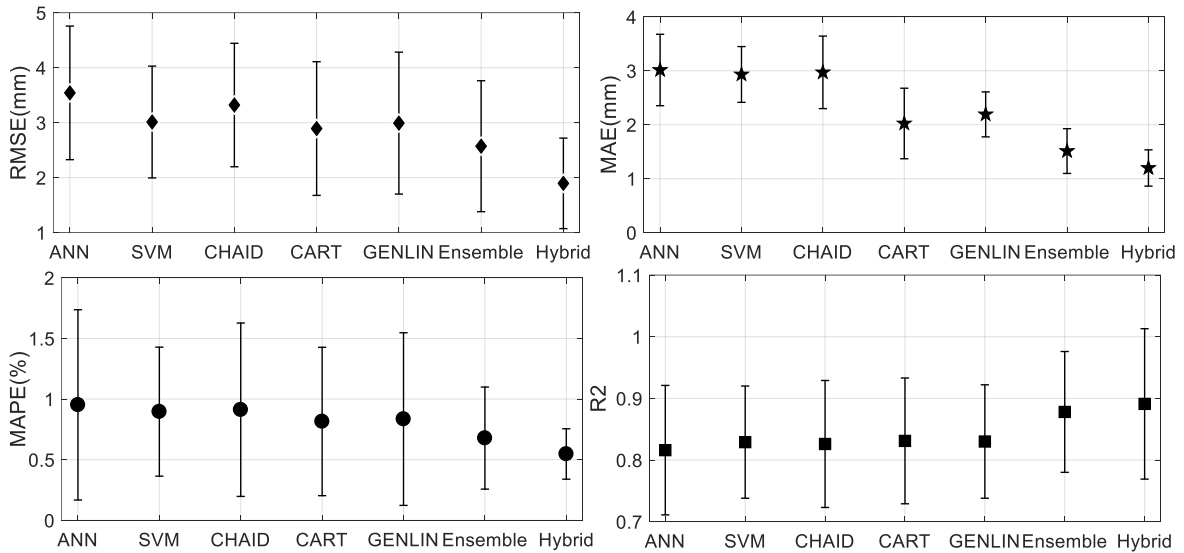
۷۳۲
۷۳۳
۷۳۴

Fig. 3. Assessing concrete strength and measuring reinforcement diameter



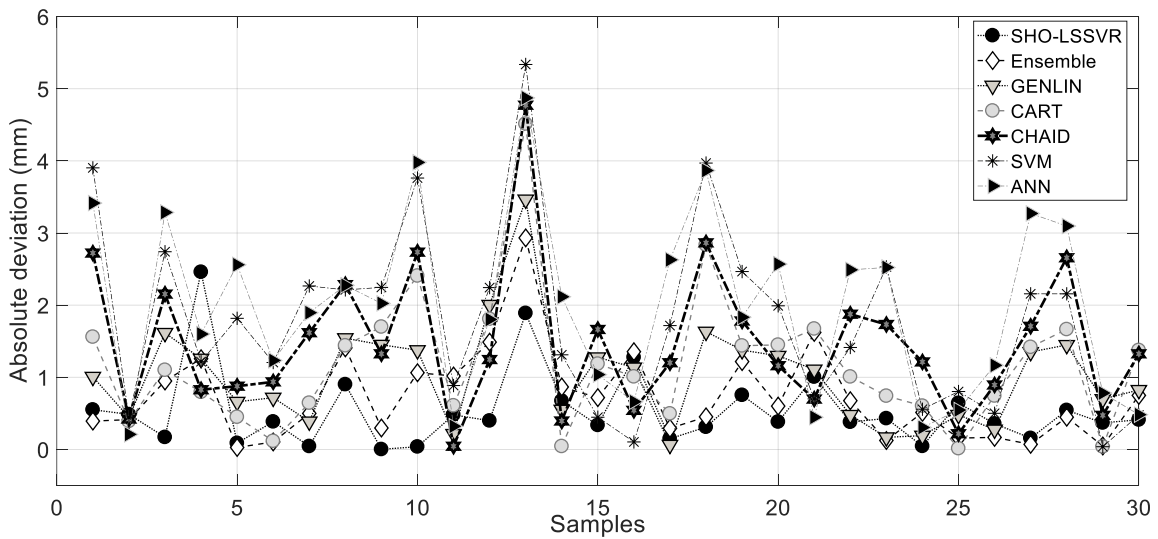
۷۳۵
۷۳۶
۷۳۷

Fig. 4. Modelling stream for predicting deflection in corroded RC beams.



۷۳۸
۷۳۹
۷۴۰

Fig. 5. Visualization of average performance results for the predictive models



۷۴۱
۷۴۲

Fig. 6. Absolute deviation for the best testing fold of all models

٧٤٣

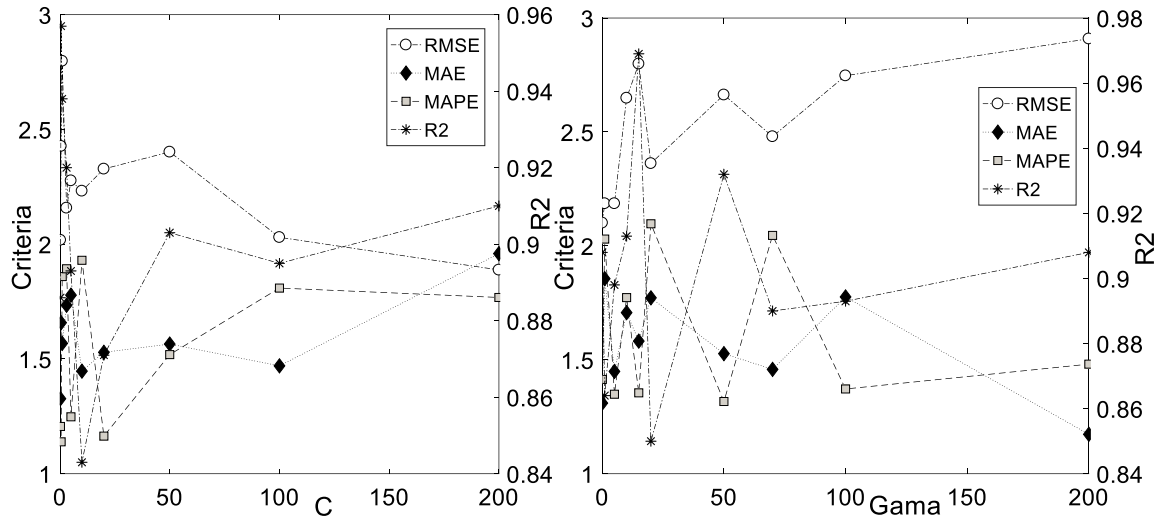


Fig. 7. Influence of model input parameters

٧٤٤

٧٤٥

٧٤٦

٧٤٧

٧٤٨

٧٤٩

٧٥٠

٧٥١

٧٥٢

٧٥٣

٧٥٤

٧٥٥

٧٥٦

٧٥٧

٧٥٨

٧٥٩

٧٦٠

٧٦١

٧٦٢

٧٦٣

٧٦٤

٧٦٥

٧٦٦

List of tables

٧٦٧ Table 1. Statistical values for all attributes 29

٧٦٨ Table 2. Settings for predictive model parameters 29

٧٦٩ Table 3. Performance of single, ensemble, and hybrid AI models for testing data 30

٧٧٠ Table 4. Average prediction results of the hybrid model across various cases 30

٧٧١

٧٧٢ Table 1. Statistical values for all attributes

Attributes	Unit	Min.	Max.	Avg.	Std.
$X1 = \text{beam length } (L)$	mm	1500	6650	4343.33	1255.12
$X2 = \text{beam width } (b)$	mm	100	1200	308.33	133.92
$X3 = \text{beam height } (h)$	mm	250	900	482.67	103.95
$X4 = \text{protective concrete cover } (a)$	mm	20.40	32.60	24.82	2.28
$X5 = \text{moment acting on the beam } (M)$	kN/m	2.01	574.29	110.42	106.82
$X6 = \text{concrete strength } (R_{bt})$	MPa	8.50	14.50	11.74	1.97
$X7 = \text{reinforcement diameter } (\varnothing)$	mm	15.00	24.90	19.19	2.86
$X8 = \text{reinforcement area } (A_s)$	mm ²	402	9420	1658.98	1387.02
$Y = \text{calculated deflection } (f)$	mm	0.38	13.48	6.01	3.76

٧٧٣

٧٧٤ Table 2. Settings for predictive model parameters

Model	Parameters	Values	Notation
Seahorse optimization	Population size	20	N_p
	Maximum iteration	25	T_{max}
LSSVR	Kernel parameter	$[10^{-5}, 10^5]$	γ
	Regularization parameter	$[10^{-5}, 10^5]$	C
SVR	Regularization parameter	10	C
	RBF gamma	0.1	γ
	Kernel type	RBF	
ANN	Transfer function	Sigmoid	
	Hidden layers	1	
	No. of neurons in the hidden layer	3	

٧٧٥

٧٧٦

٧٧٧

٧٧٨

Table 3. Performance of single, ensemble, and hybrid AI models for testing data

Model	R ²		MAE (mm)		MAPE (%)		RMSE (mm)	
	Avg.	Std.	Avg.	Std.	Avg.	Std.	Avg.	Std.
ANN (5)	0.816	0.105	3.015	0.662	0.952	0.785	3.542	1.215
SVM (3)	0.829	0.091	2.932	0.517	0.896	0.532	3.012	1.017
CHAID (4)	0.826	0.103	2.971	0.672	0.912	0.715	3.321	1.123
CART (1)	0.831	0.102	2.023	0.654	0.815	0.612	2.893	1.216
GENLIN (2)	0.830	0.092	2.192	0.417	0.835	0.712	2.992	1.291
Combined 2 best single models (CART+GENLIN)	0.878	0.098	1.512	0.415	0.678	0.421	2.572	1.191
The hybrid SHO- LSSVR	0.891	0.122	1.198	0.336	0.547	0.208	1.896	0.823

Note: The numbers in brackets indicate the ranking of the models based on their performance

Table 4. Average prediction results of the hybrid model across various cases

Case	Selected inputs for weighting	R ²		MAE (mm)		MAPE (%)		RMSE (mm)	
		Training	Testing	Training	Testing	Training	Testing	Training	Testing
Case 1	X ₁ , X ₈	0.902	0.895	2.076	2.012	2.072	2.118	2.621	2.721
Case 2	X ₁ , X ₇ , X ₈	0.892	0.897	1.982	2.008	1.962	1.912	2.608	2.708
Case 3	X ₅ , X ₆ , X ₇ , X ₈	0.906	0.911	1.543	1.812	1.672	1.832	1.982	2.246
Case 4	X ₄ , X ₅ , X ₆ , X ₇ , X ₈	0.901	0.892	1.517	1.921	1.811	1.905	2.051	2.515
Case 5	X ₁ , X ₂ , X ₃ , X ₅ , X ₆ , X ₇ , X ₈	0.912	0.905	1.427	1.732	1.342	1.517	1.912	2.365

๗๙ • **Biography:**

	<p>Duc-Hoc Tran is the associate professor of construction management at Ho Chi Minh City University of Technology, Vietnam. He studied civil engineering at Hanoi University of civil engineering from 2005 to 2010. He graduated with an MSc and PhD in Construction Management from National Taiwan of Science and Technology, Taipei, Taiwan, in 2012 and 2015. His research interests include project scheduling, scheduling theory, and intelligent optimization method, multiple objective optimization and artificial intelligence applications in construction management. He has published over 70 research papers.</p>
	<p>Thi-Cam Tien Ngo is a postgraduate candidate in construction management at Ho Chi Minh City University of Technology, Vietnam. She studied construction economics at the University of Transport and Communications from 2013 to 2017. She graduated with a Master's in Construction Management from the University of Transport and Communications, Vietnam, in 2020. Her current research interests include project costing, project scheduling, and intelligent optimization methods in construction management.</p>

๗๙๑